Global NEST Journal, Vol 24, No 3, pp 474-486

Evaluation of the performance of packed bed column for heavy metal ion removal using rice husk powder coated with iron oxide nanoparticles

Venkat Saravanan R.[1], Yuvaraja R.[1], Andal L.[1] and Yogeshwaran V.[2,*]
[1]Department of Civil Engineering, Velammal College of Engineering and Technology, Madurai, Tamil Nadu - 625009, India
[2]Department of Civil Engineering, Sri Krishna College of Engineering and Technology, Coimbatore - 641008, India
Received: 22/04/2022, Accepted: 18/07/2022, Available online: 07/08/2022
*to whom all correspondence should be addressed: e-mail: svyogi23190@gmail.com
https://doi.org/10.30955/gnj.004331

Graphical abstract

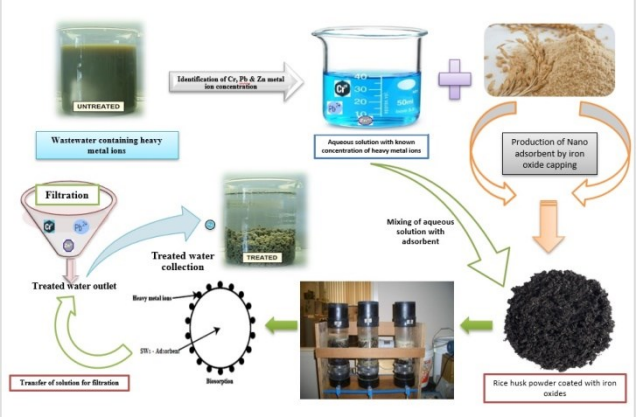

Abstract

The packed bed column study investigated the removal of toxic metal ions (Cr, Pb & Zn) using rice husk coated with iron oxide nanoparticles as an adsorbent material. The chemical fusion process prepared the nanomaterial adsorbent, and iron oxide capping provides stability to the prepared nano adsorbent. The characteristics of prepared nano adsorbents and their stability were examined by SEM/EDX, VSM, XRD, Zeta Potential, TGA & DTA methods. Breakthrough curves confirm the ability to obtain the maximum adsorption under operating conditions of 5, 7.5 & 10 - cm bed heights, 100, 200 & 300 – mg/L of metal ion concentrations and 5, 7.5 & 10 – mL/min of inflow rate of the solutions into the column. The ANOVA & CCD analysis confirms the linearity of actual and predicted values of the amount of adsorption process. Thomas and BDST model studies show the best fit to the regression values for obtaining earlier breakthroughs in the fixed bed column. At the pH of 2.0, the maximum amount of heavy metals adsorption was observed. The maximum desorption rate of the column and adsorbent material was obtained by adding 0.3 N of H_2SO_4 at 40 minutes average time for all the three metal ions.

Keywords: Fixed bed column, rice husk, nano-adsorption, iron oxides, desorption

1. Introduction

Eliminating toxic heavy metal ions (Cr, Pb and Zn) in the industrial effluent is critical and requires additional treatment apart from the primary, secondary and biological treatment process. The industrial effluent has various types of heavy metal ions, which creates poisonous effects due to the direct discharge from the industries without any prior treatment. It is necessary to remove/reduce the toxic contaminants in the effluent as a part of mitigation measures (Singha *et al.*, 2011). Many treatment techniques are available to eliminate the toxic pollutants from their source of accumulation. But all those additional treatment technologies require very high capital and investment cost, skilled workers, large space etc., Also, it produces a high amount of secondary sludge, and using highly concentrated acids/chemicals is a major disadvantage (Yogeshwaran *et al.*, 2021). Adsorption is one of the treatment techniques used widely in recent days to remove/reduce the concentrations of toxic pollutants. It is the process that can accumulate the pollutants on the surface of the adsorbent material (Hasfalina *et al.*, 2012). Normally, the adsorbent material is created using organic decomposable wastes such as grape leaves, neem leaves, date seeds, rice hulls etc., (Hezagi *et al.*, 2013). The adsorbent materials are synthesized and converted into activated carbon to obtain more surface area and pollutants onto the adsorbent surface (Priya *et al.*, 2022). This happened due to the Van Der – Walls force between the inner walls of the adsorbent surface and the pollutants (Yunnen *et al.*, 2017). The process of adsorption may be done by batch/column mode of study based on the concentrations of pollutants.

Due to the variations in metal ion concentrations and unpredictable flow rates, the batch mode of adsorption has not been able to provide a good quality of results (Wolowiec *et al.*, 2019). For the large-scale treatment process, the fixed bed columns are most suitable to

operate in continuous flow mode. It is very easy to operate and provides good quality results for the large volume of effluents. Most of the experimental study reports suggested the packed bed column mode of the adsorption process for maximum efficiency (Nadaffi *et al.*, 2007). Nano-adsorption is the new emerging technology used to eliminate the toxic pollutants up to the nanoscale range (10-9 mm) in the effluent (Goharshadi *et al.*, 2015). Hence it was decided to convert the rice hulls into nanoscale range by chemical synthesis process and planned to use that as an adsorbent material in packed bed column. Converting the organic material from mm to nm is complicated, and its stability is not good (Luyen *et al.*, 2019). Due to water content in organic material, the stability during the treatment process is not good. To increase the stability of organic nanoparticles, need to provide any capping process using iron oxide, zinc oxide, titanium oxide etc. (Khulbe *et al.*, 2018). The iron oxide capping process is simple to increase the stability of nanoparticles and provides sufficient temperature resistance to the adsorbent material (Ali Kara *et al.*, 2013). Based on the above discussions, we decided to eliminate the toxic pollutants from the effluent using a nano-adsorption process in a packed bed column. Here, the rice hulls were used as an adsorbent material to receive the chromium, lead and zinc metal ions from the aqueous solutions.

2. Materials and methods

2.1. Materials

2.1.1. Preparation of rice hull adsorbent & stock solution

Rice hulls are the protective shells of rice that were collected in local rice mills at Coimbatore district, Tamilnadu, India. The collected rice hulls are washed thoroughly with double distilled water to remove the impurities and dust particles. Then the washed rice hulls were kept and dried in the sunlight for up to 24 hrs. The dried rice hulls were placed in a muffle furnace at 150°C for 3 hours. The rice hulls are taken from the muffle furnace, washed with concentrated sulfuric acid to remove the organic and biological pollutants, and filtered by Whatman's filter paper further; it dries in sunlight. Finally, the dried rice hulls were taken for experimental work with a size range of 125–150 µm. The stock solutions were prepared by adding potassium dichromate (K2Cr2O7), Zinc Chloride (ZnCl2) and Lead Sulphate (PbSO4) with distilled water in the ratio of 1:10 by weight and the solution was kept under a controlled tempera-ture. The concentrations were obtained at various levels by design using the double-distilled water, and the pH adjustments were done by adding concentrated sulfuric acid (0.1 M).

2.1.2. Iron-oxide capping process of the adsorbent

10 mL of distilled water was taken, and ferrous sulfate heptahydrate ($FeSO_4{\cdot}7H_2O$) and ferric chloride hexa-hydrate ($FeCl_3.6H_2O$) were mixed with the distilled water with the ratio of 1:2 with the Fe^{3+} and Fe^{2+} salt concentrations of 1.5:1. Then the sample was heated up to 100°C by the magnetic stirring method. Further, the ammonia solution was mixed with the heated solution, and the mixing process was continued. 15 gm of ground rice hull powder was added to the solution for the capping process (Venkatraman *et al.*, 2022). To maintain the equilibrium mixing, the continuous stirring was done for up to 30 minutes and kept the solution in a muffle furnace at the temperature of 100°C. For the separation of black precipitates on the adsorbent, the sample was taken from the furnace and washed with the ethanol solution followed by distilled water (Buthelezi *et al.*, 2012). Using the magnetic separation process, the waste residuals in the iron oxide particles were removed, and the final solution was kept in an oven at 80°C for drying. The dried adsorbent was taken from the oven and used for further experimental studies.

2.2. Methods

2.2.1. Characterization of rice hulls capped with iron oxides

FTIR studies

The connection between hydroxyl and carbonyl functional groups has been considered in this method to examine the characteristics of meal ions adsorbed by the rice hulls powder coated with iron oxides. Here, 0.5 gm of iron oxide coated rice hulls powder was taken and mixed with 50 mg/L of solution with heavy metals of Cr, Pb and Zn & the pH was adjusted to 6.0 by adding distilled water for dilution in a conical flask. The supernatant was filtered out after 5 hours of constant rotating speed (200 rpm). For the spectrum (IR) attainment, 2 mg of rice hulls coated with iron oxide particles were finely grouted with the KBr pellets of 250 mg. For obtaining the spectra, the FTIR spectrophotometer was used with the range of scanning interval adjusted from 400 – 4000 cm^{-1} for 20 scans with a resolution of 4 cm^{-1}.

SEM & EDX analysis

Scanning Electron Microscopic (SEM) analyses were performed under a working distance of 15 kV to evaluate the flaws, fractions on the adsorbent surface and contaminants. Using the Brucker – EDX system, the analysis of the elements and metal ions & their distribution was investigated based on the methodology suggested in the previous publications.

XRD analysis

X-ray diffraction is used to determine the crystalline structure of the prepared rice hulls nanoparticles coated with iron oxides. The XRD analysis was performed under various conditions to check the properties of synthesized rice hulls nanoparticles. With 250 mA & Cu -K α radiation, the X-Ray Diffractometer was operated to find out the size of the crystalline & its phases. The peaks obtained from the XRD analysis have been compared with the JCPDS reference standards (Joint Committee on Powder Diffraction Standards – 00 -002- 1035).

Zeta potential analysis

The prepared rice hull nanoparticles were subjected to ZPA analysis to determine the surface charge and stability. The surface charge and stability are the important property of nanoparticles to find out how they are stable during the suspension and repulsion between the particles (Pandey *et al.*, 2017). When the ZPA values are very high, it indicates

the accumulation between the prepared nanoparticles and their unstable nature. This is because of the very high surface area of the nanoparticles and other major properties.

TGA & DTA analysis

Thermogravimetric analysis checks the changes in the nanoparticles and their mass during the heating process. The nature of the reaction (Endothermic/Exothermic) was verified by the differential thermal analysis at which temperature the reaction happened (Samir *et al.*, 2011). The experimental procedure was done under the air with 20 mg of the sample placed in the instrument.

2.2.2. Fixed bed adsorption studies

For fixed-bed experimental work and analysis, a glass column was taken with an internal diameter of 2 cm and an overall length of 30 cm, as shown in Figure 1. The parameters of the fixed bed column (depth of bed, flow rate & metal ion concentrations) have been varied under standard conditions to evaluate the performance of the fixed bed column. The depth of the adsorbent (Rice hulls coated with iron oxides) bed was adjusted as 5, 7.5 & 10 cm, the flow rate of the metal ion solution was adjusted as 5, 7.5 & 10 mL/min, and the concentration of heavy metal ions (Cr, Pb & Zn) was adjusted as 100, 200 & 300 mg/L for the entire analysis which was used to obtain the breakthrough curves of the fixed bed column studies. Form equilibrium studies of the adsorption process, Thomas and Yoon – Nelson model studies were performed. To perform the desorption studies, concentrated sulfuric acid by varying the normality (0.1, 0.2 & 0.3) was used, and the adsorbed metal ions were disposed of by remote landfilling method.

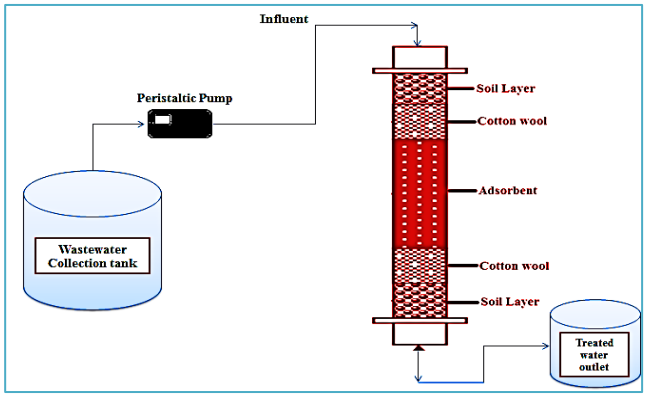

Figure 1. Experimental setup of fixed bed column.

To perform the breakthrough analysis of the fixed bed column the following equations (2.1 to 2.5) were used.

$$q_{total} = \frac{Q}{1000}\int_{t=0}^{t_{total}} C_{ad}\,dt \tag{2.1}$$

$$V_t = Qt_{total} \tag{2.2}$$

$$q_{bed} = \frac{q_{total}}{W} \tag{2.3}$$

$$M_{total} = \frac{C_0 Q t_{total}}{1000} \tag{2.4}$$

$$\%removal = \frac{q_{total}}{M_{total}} * 100 \tag{2.5}$$

Where,

q_{total} – Total weight of metal ions adsorbed by the adsorbent in fixed bed column in mg

C_o – Initial metal ion concentration (mg/L)

C_{ad} – Initial and final metal ion concentration difference at the end of flow time in (mg/L)

V_t – Volume of treated effluent

Q – Volumetric flow rate (mL/min)

T_{total} – Total flow time

q_{bed} – Capacity of the bed (mg/g)

W – Weight of the adsorbent (g)

M_{total} – Total amount of metal ions added in the column

% Removal – Total metal ions removal

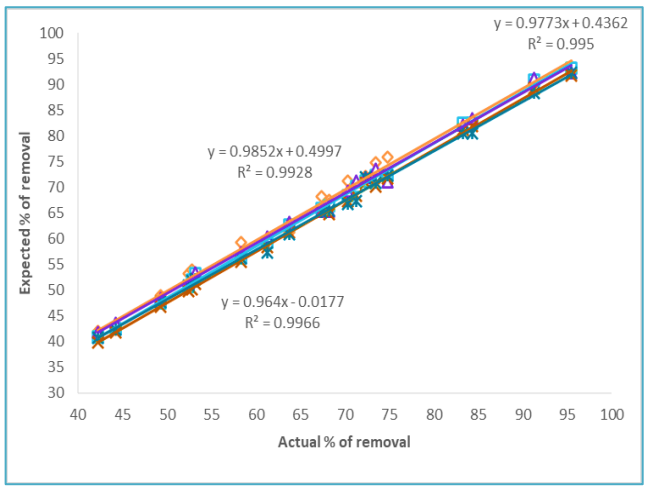

Figure 2. Variation of estimated Cr, Pb & Zn metal ion removal values vs. Measurements.

2.2.3. Central composite design

The heavy metal ions interactions and the experimental variable effects have been calculated by using the Central Composite Design (CCD) analysis. To find out the optimum points, the CCD used 20 runs which include factorial points (08), axial points (06) and center points (06). The certain investigational constraints and their values are represented in Table 1. To avoid precipitation, the actual pH values are maintained for all experiments. The metal ion removal and its relationship with the adsorption factors were obtained with coded variables as follows (Equation 2.6–2.8). Figure 2, shows the relationship plot between the expectation and prediction adsorption values of Cr, Pb and Zn metal ions, respectively.

For Cr (VI) removal (%)

$$Y = 48.05 - 15X + 0.13Y + 4.75Z - 1.25XY + 0.35XZ + 1.02YZ + 2.89X^2 - 0.15Y^2 + 1.4Z^2 + 0.65XYZ \quad (2.6)$$

For Pb (II) removal (%)

$$Y = 28.75 - 7.25X + 1.34Y + 1.9Z - 2.08XY + 0.15XZ + 3.76YZ + 3.73X^2 + 0.75Y^2 - 0.53Z^2 - 1.73XYZ \quad (2.7)$$

For Zn (II) removal (%)

$$Y = 82.95 - 4.66X + 2.06Y - 0.44Z + 2.04XY + 5.73YZ + 6.33XZ - 9.26X^2 + 1.2Y^2 + 0.33Z^2 + 0.56XYZ \quad (2.8)$$

Where,

X – Coefficient of heavy metal ion in initial concentration

Y – Coefficient of time

Z – Coefficient of adsorbent dosage

The sustainability and significance of the developed model have been examined by the Analysis of Variance (ANOVA) tools and represented in Table 2, which indicates the metal ion removal (Cr, Pb and Zn) to calculate the response of initial metal ion concentration (mg/L), time of removal (s) and adsorbent dosage (gm). The lack of fit (F) of the design for Cr (VI), Pb (II) and Zn (II) metal ions adsorption were 46.82, 40.10 and 43.18, respectively. This indicates the models were substantial and suitable; there was a chance for a 0.01% change in Cr and Pb adsorption and 0.02% in Zn adsorption that the lack of fit (F) values could sustain. For Chromium (Cr) removal, the lack of fit (F) value is 0.26, which indicates that it was not relatively significant to the pure error. Similarly, for Lead (Pb) and Zinc (Zn) metal ion removal, the 'F' values of 0.19 and 0.21 indicate that they were not comparatively substantial to the pure error and that the quadratic models were valid for the present study (Sukumar *et al.*, 2016). A lack of non-significant fit was considered good to fit the model. In Table 2, the regression values (R^2) are found to be 0.9871, 0.9840 and 0.9763 for Cr (VI), Pb (II), and Zn (II) metal ion removal, which indicates the values are between 0 to 1 ($0 \le R^2 \le 1$). The square root of the variance is represented in the standard deviation quantity. The new experiment's responses can be predicted using the Predicted Residual Sum of Squares (PRESS) criterion for the model's efficiency. The smaller levels of PRESS are more suitable. Table 2 represents the ANOVA values, X – Metal ion concentration (mg/L), Y – Time of removal (s) and Z – adsorbent dosage.

2.2.4. Response surface methodology

The response surface plots for the impact of pre-metal ion concentration, the quantity of adsorbent and interaction between time for Cr (VI), Pb (II) and Zn (II) metal ion removal as shown in Figures 3 and 4. Referring to Figure 3, the impact of time of removal was not difficult for improving the adsorption volume of the nano-adsorbent. Still, the heavy metal ion concentration strongly impacted adsorption efficiency (Fenglian Fu *et al.*, 2011). The figure identified that with the initial metal ion concentration moving through at a constant time, the amount of adsorption efficiency decreased dramatically. Also, in Figure 4, the removal efficiency of Pb (II) ions has decreased slowly after the saturation point since the metal ions covered the active sites (Barakat, 2011). A similar trend was seen in Figure 4 for Cr (VI) and Zn (II) ions with an increase in concentration after the saturation level.

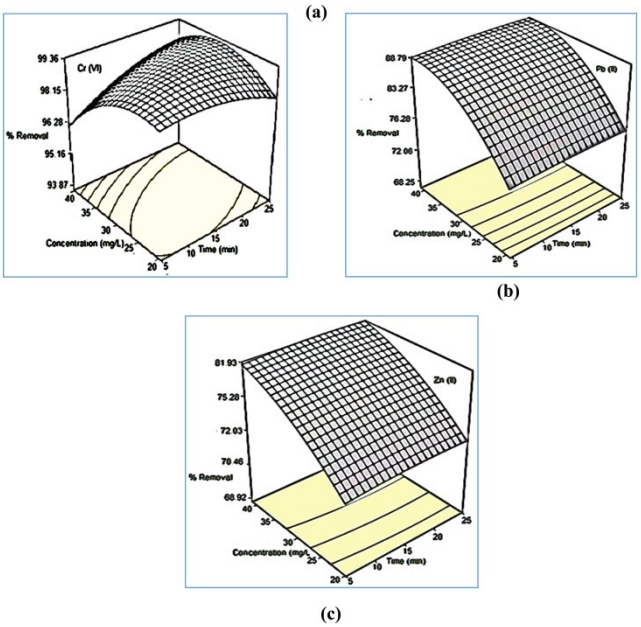

Figure 3. 3D surface plots for the impact of (a) Cr, (b) Pb & (c) Zn metal ion removal and metal ion concentrations with respect to time.

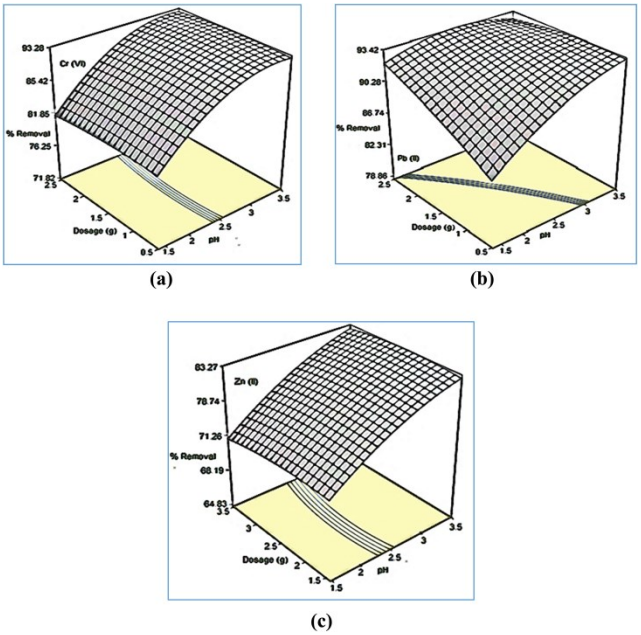

Figure 4 3D surface plots for the impact of (a) Cr, (b) Pb & (c) Zn metal ion removal and adsorbent dosage with respect to pH.

On the other hand, the efficiency of the adsorption process was increased with an increase in adsorbent dosage, as shown. The volume of adsorbent is very high, and it raises the adsorbing surface that the attractively active surfaces prepare some surfaces for adsorbing metal ions (Ashraf Ali *et al.*, 2016). Due to the external surface adsorption process, the quick adsorption is attributed to rice hulls adsorbent coated with iron oxide nanoparticles (Priya *et*

al., 2022). The adsorption sites of iron oxide-coated nanoparticles can be found on the external surface of the adsorbent, and these active sites attract the metal ions; thus, the equilibrium has been attained rapidly (Nilisha *et al.*, 2013). The optimum conditions of heavy metal ion removal were obtained using the software and represented in Table 3. It confirms that both the experimental and predicted results were in good agreement.

Due to the differences in ionic radius of Cr (VI), Pb (II) and Zn (II), the efficiency of adsorption results shows the difference. The heavy metal ion removal efficiency followed the increasing order: Cr (VI) > Pb (II) > Zn (II). Compared to Cr (VI) (2.0 Å) and Pb (II) (1.32 Å) metal ions, the radius of Zn (II) (0.73 Å) is very small, which is formed a water layer of very large size on the adsorbent surface. As a result, Zn (II) is more mobile in bulk solution and would have a smaller propensity to adsorb on the rice hulls nano-adsorbent.

Table 1. Design matrix for experimental and predicted removal of metal ions obtained by CCD

Trial No.	Pre - metal ion concentration (mg/L)	Removal Time (s)	Dose Level (gm)	Removal of Cr (VI) (%)		Removal of Pb (II) (%)		Removal of Zn (II) (%)	
				Exp.	Pre.	Exp.	Pre.	Exp.	Pre.
1	100	40	0.25	53.23	51.73	53.21	53.43	51.25	52.13
2	200	20	1	67.41	68.26	65.82	65.26	65.28	65.16
3	100	120	0.75	83.25	82.17	82.48	82.18	81.21	80.46
4	200	80	1	72.35	72.18	71.27	71.89	70.82	71.93
5	100	120	1.25	91.27	90.21	90.83	91.25	89.23	88.36
6	100	40	1.25	84.33	82.28	82.46	83.29	81.85	80.53
7	50	80	1	95.46	93.54	93.27	92.24	91.84	92.28
8	200	80	0.75	70.28	71.27	68.46	69.28	67.36	66.83
9	200	80	1.25	73.46	74.72	72.28	73.56	70.21	70.83
10	200	80	0.5	58.28	59.34	56.26	57.29	55.54	56.27
11	300	120	1.25	52.46	53.28	50.65	51.28	49.89	50.82
12	300	40	1.25	49.28	48.92	47.45	48.46	46.83	47.73
13	200	80	1.5	61.28	59.28	59.25	60.29	58.38	57.26
14	300	120	0.75	52.83	53.83	51.93	52.21	50.16	51.83
15	350	80	1	42.25	41.98	40.83	41.74	39.82	40.63
16	250	80	1	63.72	61.29	62.62	63.28	61.28	60.82
17	300	40	0.75	44.27	42.34	42.46	43.65	41.84	42.39
18	200	150	1	74.82	75.93	72.28	71.08	71.75	72.38
19	200	40	1	68.26	67.43	66.33	65.38	64.82	65.56
20	200	80	1	71.28	70.04	70.18	71.25	68.45	67.37

Table 2. ANOVA for quadratic model for removal of Cr (VI), Pb (II) and Zn (II)

Source	Adsorption of Cr (VI) (%)			Adsorption of Pb (II) (%)			Adsorption of Zn (II)		
	Mean square	Value of F	Value of p	Mean square	Value of F	Value of p	Mean square	Value of F	Value of p
Model	345.97	46.82	0.0001	251.95	40.10	0.0001	324.92	43.18	0.0001
X	3608.99	471.41	0.0001	1873.83	298.28	0.0001	3246.73	389.29	0.0001
Y	0.19	0.032	0.8286	423.79	63.79	0.0001	0.18	0.0023	0.7869
Z	308.84	45.12	0.0001	14.87	2.63	0.5981	285.37	43.29	0.0001
XY	12.50	1.70	0.2248	113.21	17.59	0.1643	11.29	1.46	0.2123
XZ	1.31	0.17	0.7029	64.64	10.64	0.0031	1.18	0.13	0.6892
YZ	8.28	1.19	0.3423	158.70	25.51	0.0121	7.46	1.12	0.2832
X^2	124.75	17.23	0.0026	172.39	26.72	0.0012	112.85	14.92	0.0021
Y^2	0.24	0.031	0.8607	548.34	86.96	0.0009	0.18	0.025	0.8329
Z^2	25.76	3.57	0.0893	27.14	4.73	0.0001	26.25	4.28	0.0832
XYZ	3.32	0.46	0.5408	265.85	43.23	0.0683	3.18	0.39	0.4725
Residual	7.63	--	--	6.72	--	--	7.28	--	--
Lack of fit	2.65	0.26	0.9511	1.75	0.19	0.9223	2.28	0.21	0.9326
Pure error	11.40	--	--	9.30	--	--	10.21	--	--
Standard deviation		2.64			2.37			2.04	
PRESS		216.77			246.82			205.28	
R^2		0.9871			0.9840			0.9763	
Adjusted R^2		0.9631			0.9650			0.9594	
Predicted R^2		0.9493			0.9539			0.9338	
Adequate precision		25.792			23.648			24.273	

Table 3. Optimum conditions for metal ion (Cr, Pb & Zn) removal

S. No.	Metal ions	Pre metal ion concentration (mg/L)	Removal time (min)	Adsorbent dosage (g)	pH	Removal (%)			
						Actual	Predicted	Error	Std. Dev.
1.	Cr	25	15	1.5	2.5	99.36	99.58	0.22	0.05
2.	Pb	25	20	1.5	3	88.79	89.25	0.46	0.09
3.	Zn	25	20	2.5	2.5	81.93	82.67	0.74	0.16

2.2.5. Thomas model

The Thomas model for column evaluation evaluated the BT (Break Through) curves and their prediction. In the adsorbent bed, the predominance of the plug flow dispersion occurred. This is the elementary statement of the Thomas model, and the equation for this model is expressed as (Equation 2.9).

$$\ln\left(\frac{C_o}{C_i}-1\right)=\frac{K_{th}q_o w}{Q}-K_{th}C_o t \quad (2.9)$$

The Thomas model constraints 'K_{th}' 'q_0' were obtained by intrigue ln $((C_o/C_i) - 1)$ vs. time and the slope were obtained by multiplying K_{th} and C_o & Intercept was taken by

$$\text{Intercept}=\frac{K_{th}q_o W}{Q}$$

The Thomas model constraints 'K_{th}' 'q_o' were obtained by intrigue ln $((C_o/C_i) - 1)$ vs. time, and the slope was obtained by multiplying Kth, and Co & Intercept was taken by

2.2.6. Bed depth service time (BDST) – model

By predicting various breakthrough points, the adsorbent bed capacity was obtained. The surface reaction occurred on the surface of the adsorbent, and the BDST model assumes that the unused capacity of the adsorbent was controlled throughout the entire adsorption process. The parameters of the BDST model (No & K) were obtained by plotting the gph of bed depth vs. time, and the equation of this model can be expressed as (Equation 2.10).

$$t=\frac{N_0 Z}{C_o V}-\frac{1}{KC_0}\ln\left(\frac{C_o}{C_b}-1\right) \quad (2.10)$$

Where the service time of the column is denoted by t in minutes, the capacity of the adsorbent bed is represented as No in mg/L, Column bed depth is represented as Z in cm, Concentration of the influent solution is represented as C_o in mg/L, Linear flow velocity is represented as V in cm/min, metal ion breakthrough Concentration is represented as C_b in mg/L, and the rate constant is represented as K in L/mg. min.

3. Results and discussion

3.1. FRIR studies

Figure 5 shows the FTIR spectrum of the rice hulls powder adsorbent coated with the iron oxides for raw and metal ions loaded powder. The maximum peak was attained at 3430 cm^{-1} because of the alcohol groups and the stretching vibration of water. The existence of aromatic rings provides the stretching vibration of –C–H at the peak of 3092 cm^{-1} and ring vibration at 1602 and 1456 cm^{-1}. Another peak was recorded at 1621 cm^{-1}, which is assigned to C=O because of the presence of the carbonyl group. The peaks at 1320, 1367, 1326 and 1463 cm^{-1} confirm bending vibrations by -CH_2. The fine structure may be obtained because of hydrogen bonding in the region with no energy (Samson *et al.*, 2016). The peak from 3472 cm^{-1} to 3357 cm^{-1}, 3393 cm^{-1} and 3367 cm^{-1} shows the vibration stretching of alcohol and 1627 cm^{-1} to 1619 cm^{-1}, 1548 cm^{-1} and 1518 cm^{-1} shows the vibration stretching of C=O. Then, the peak of disappearing approves the existence of esters due to C-O strong stretching at 1210 cm^{-1}.

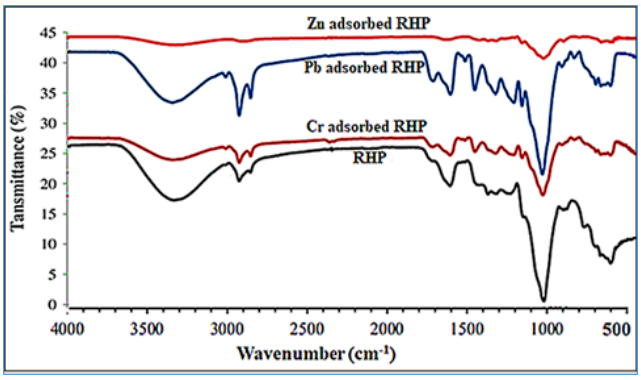

Figure 5. FTIR spectrum of rice hulls adsorbent coated with iron oxides.

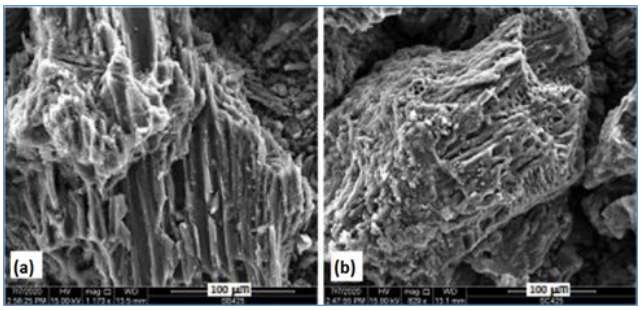

Figure 6. SEM image of rice hulls adsorbent coated with iron oxides.

3.2. SEM/EDX analysis

The microscopic images of iron oxide-coated rice husk powder before and after the adsorption of heavy metal ions is shown in Figure 6. By referring the Figure 6, it was seen irregular shapes on the surface of rice husk powder due to acid treatment. The nano-adsorbent can adsorb the toxic pollutants from the aqueous solutions after seeing the SEM image. The process of adsorption has been completed by filling the porous surface of the rice husk power with toxic and other pollutants. The heavy metals were adsorbed in the innermost walls of the adsorbent surface and loaded heavily (Rai *et al.*, 2016). The EDX image (Figure 7) of the metal ion adsorbed adsorbent confirms the adsorption of heavy metal ions (Cr, Pb and Zn) along

with other organic and inorganic pollutants such as Sulphur, Carbon & Magnesium etc.

The hydroxyl groups in the rice husk powder react with the concentrated sulfuric acid during the treatment process and produce the sulfate esters. It acts like a non-alcoholic group by complex citations (Lalitha *et al.*, 2018). Based on the above observations, the concentrated sulfuric solution has not destroyed any significant functional groups of rice husk adsorbent, and it protonates the charged sites.

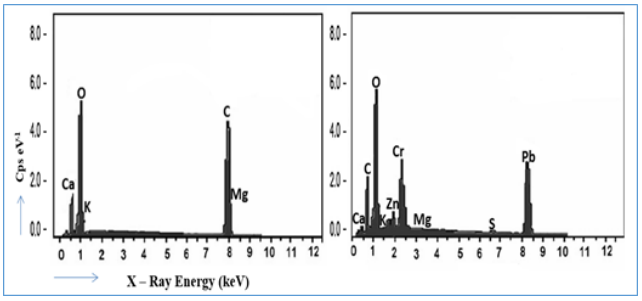

Figure 7. EDX image of rice hulls adsorbent coated with iron oxides.

3.3. XRD analysis

The rice husk powder coated with iron oxides shows a very high intensity and crystalline structure at the various peaks (Figure 8). The hkl planes of 220, 311, 400, 422, 511 and 440 with 2θ match the peak characteristics of 300, 350, 430, 530 and 620 for the rice husk powder coated with iron oxides. Hence, it confirms the adsorbent's high-pitched diffraction points based on the crystal's nature (Sathish *et al.*, 2015).

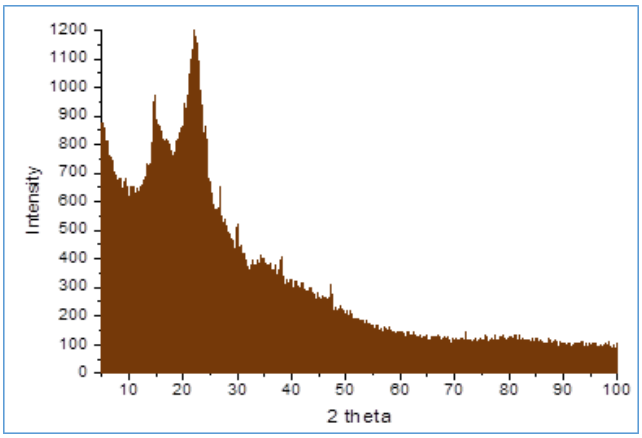

Figure 8. XRD pattern of rice hulls adsorbent coated with iron oxides.

3.4. Zeta potential analysis

A higher value was obtained (-23.9 mV) with good quality for the rice husk powder coated with iron oxides by zeta potential analysis (Figures 8 and 9). On the other hand, the carboxylate group's (COO-) presence was observed by indicating negatively charged iron oxide nanoparticles and their bonding. Hence, the adsorbent has a surface charge and stability in the high range (Akpen *et al.*, 2018).

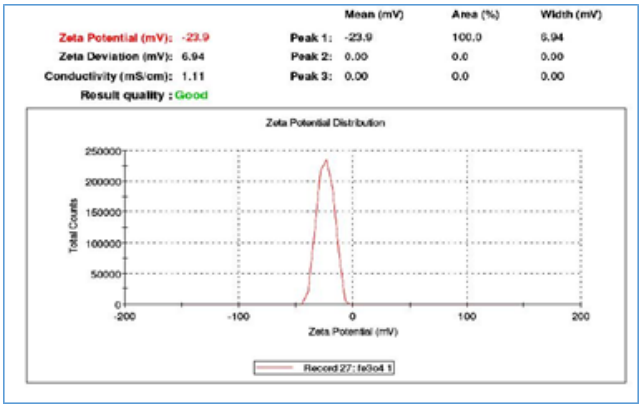

Figure 9. ZPV of rice husk adsorbent with iron oxides.

3.5. TGA & DTA analysis

The rice husk coated with iron oxide samples was subjected to heating up to 800°C with the rate of 10°C/min, and the rate of decomposition was observed at two stages (TGA & DTA). The sample dehydration process creates the weight loss of the samples, and above 600°C, the sample creates evaporation (Figure 10). The iron oxide nanoparticles and their presence were observed at the saturation point of 800°C, which confirms the success capping of iron oxides with rice husk powder.

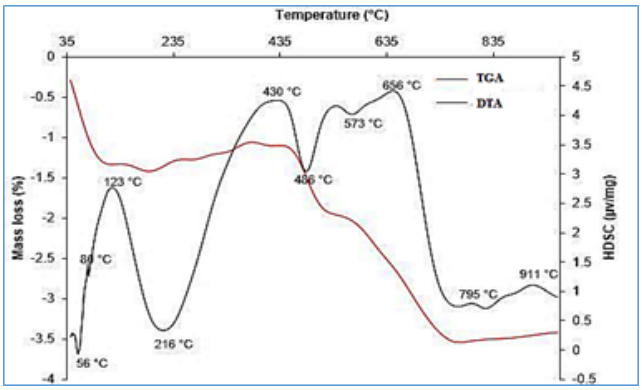

Figure 10. TGA & DTA analysis of prepared nano adsorbent.

3.6. Breakthrough analysis

The breakthrough study of the fixed bed column was studied by adjusting the parameters of heigh of the adsorbent bed, inflow rate of the metal ion solution and varying the concentrations of metal ions. These experimental works were conducted to obtain the maximum efficiency with the optimum level of the parameters. On a trial-and-error basis, the adsorbent bed height was initially adjusted at 5, 7.5 and 10 cm levels and kept the other parameters constant. i.e., metal ion concentration is 100 mg/L and inflow rate is 5 mL/min. The inflow and outflow concentrations of the metal ion solutions were tested in gradual intervals and presented in graphical representation (Figure 11). Varying the bed height of the adsorbent from 5 to 10 cm, a sharp curve was developed for Cr, Pb and Zn metal ion adsorption, and the exhaust time also increased. At10 cm bed height, the innovation time was attained, and the staying time of the inlet solution on the adsorbent bed has increased the adsorption rate also. Furthermore, the active binding sites may be increased for the adsorption of pollutants.

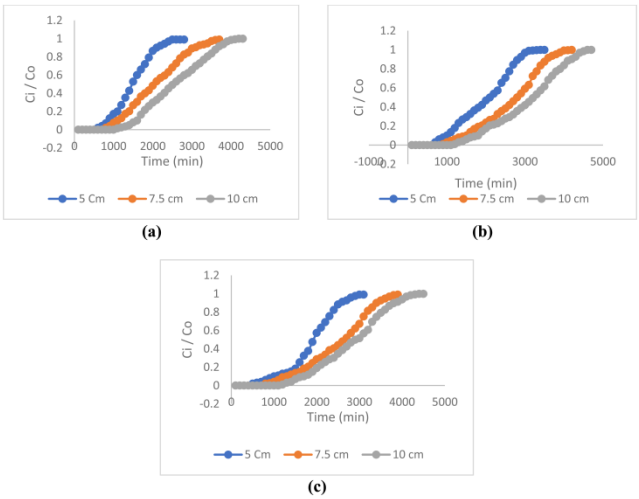

Figure 11. Break through curve at different bed depths for metal ions (Cr, Pb and Zn) adsorption.

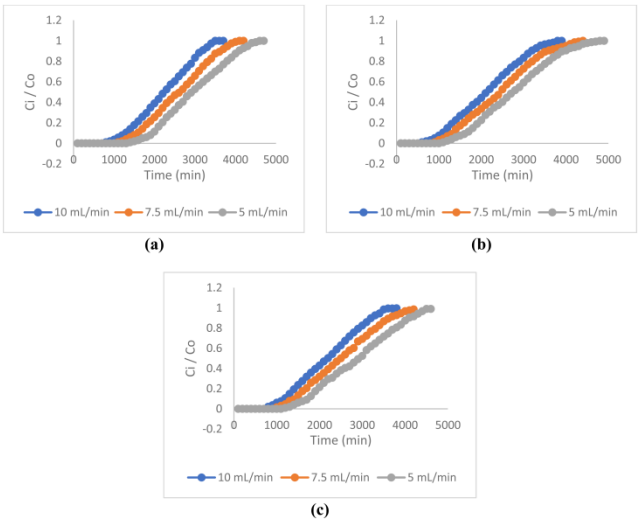

Figure 12. Break through curve at different flow rates for metal ions (Cr, Pb and Zn) adsorption.

The breakthrough through height of the column was obtained at 10 by referring to previous experimental analysis and observations. The adsorbent bed height was fixed at a 10 cm level for further experimental process. By keeping the concentration of metal ions at a constant level (100 mg/L), the breakthrough time of the flow rate of the column was obtained by varying the inflow rate of the solutions. i.e., 5 mL/min, 7.5 mL/min & 10 mL/min respectively. The metal ion adsorption is inversely proportional to the inflow rate of the solution in the column. The above-said theorem confirms that the breakthrough time of the column was attained at 5 mL/min of the inflow rate of the metal ion solution (Figure 12). Here, the breakthrough time was attained at the earlier stage to lead to the quick saturation of metal ions on the surface of the rice husk adsorbent material (Chen *et al.*, 2016). This is because of turbulence flow of the solution at a very high flow rate also decreases the mass transfer from other sources (Edokpayi *et al.*, 2015).

The above experimental work confirms the breakthrough time was attained at 10 cm bed height and inflow rate of 5 mL/min for the fixed bed column. Taking these values as constant and varying the metal ion concentrations at 100, 200 & 300 mg/L, the breakthrough time was examined. In this experimental work, many effluents play a vital role, and the breakthrough time was not attained in the initial stages with a low concentration of solutions. The diffusion coefficient level is decreased due to the gradient development in the lower concentrations, and the rice husk adsorbent recognizes the transport of heavy metal ions on the surface at a very slow rate (Figure 13). A quick saturation of the adsorbent bed was observed at the initial stages with higher concentrations of metal ions for attaining the fast breakthrough. The decrease in metal ion concentration increases the amount of adsorption by driving forces in the mass transfer zone (Guo *et al.*, 2018). Tables 4–6 provides the complete breakthrough data for varying the adsorbent bed height, Inflow rate & Metal ion concentrations, respectively.

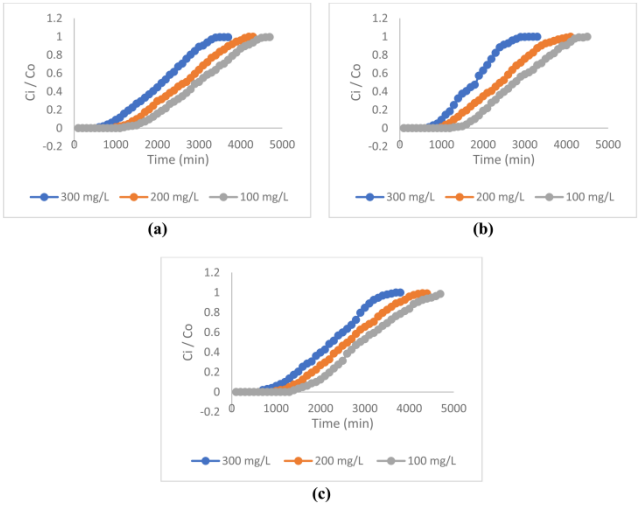

Figure 13. Break through curve at different concentrations for (a) Cr, (b) Pb & (c) Zn metal ion solutions.

Table 4. Analysis of breakthrough in various adsorbent bed heights

S.No	Type of Metal	Bed depth, Z (cm)	t_b (min)	V_t (mL)	T_{total} (min)	M_{total} (min)	q_{total} (mg)	q_{bed} (mg/g)	% Removal
1.	Cr (VI)	5	500	14000	2800	1400	1085.3	223.72	77.59
2.		7.5	700	18500	3700	1850	1526.2	289.26	82.57
3.		10	1000	21500	4300	2150	1887.7	347.63	87.84
4.	Pb (II)	5	600	17500	3500	1750	1034.2	203.36	59.18
5.		7.5	800	21000	4200	2100	1385.8	258.25	66.04
6.		10	1100	23500	4700	2350	1666.1	317.62	70.95
7.	Zn (II)	5	400	15500	3100	1550	1236.6	213.72	79.78
8.		7.5	700	19500	3900	1950	1661.4	279.35	85.24
9.		10	1100	22500	4500	2250	2000.2	335.43	88.97

Table 5. Analysis of breakthrough in various inflow rate of the solution

S.No	Type of Metal	Flow rate (Q) (mL/min)	t_b (min)	V_t (mL)	T_{total} (min)	M_{total} (min)	q_{total} (mg)	q_{bed} (mg/g)	% Removal
1.	Cr (VI)	5	1300	23500	4700	2350	1935.2	395.04	82.36
2.		7.5	1000	31500	4200	3150	2495.7	300.97	79.23
3.		10	700	37000	3700	3700	2875.6	225.3	77.72
4.	Pb (II)	5	1100	24500	4900	2450	1745.3	348.88	71.24
5.		7.5	800	33000	4400	3300	2271.7	302.72	68.84
6.		10	500	39000	3900	3900	2618.8	224.83	67.15
7.	Zn (II)	5	1100	23000	4600	2300	1884.3	376.46	80.19
8.		7.5	900	31500	4200	3150	2465.8	299.24	78.28
9.		10	700	38000	3800	3800	2932	214.89	77.16

Table 6. Analysis of breakthrough in various metal ion concentrations

S.No	Type of Metal	Ion Conc. (C_0) (mg/L)	t_b (min)	V_t (mL)	T_{total} (min)	M_{total} (min)	q_{total} (mg)	q_{bed} (mg/g)	% Removal
1.	Cr (VI)	100	1100	23500	4700	2350	1900.1	365.4	80.85
2.		200	900	21500	4300	4300	3280.9	436.8	76.32
3.		300	500	18500	3700	5550	3966.5	495.3	71.47
4.	Pb (II)	100	1200	23000	4600	2300	1670.2	340.8	72.62
5.		200	900	21500	4300	4300	2985.4	439.6	69.43
6.		300	600	16500	3300	4950	3309	378.1	66.85
7.	Zn (II)	100	1300	24000	4800	2400	1950	410.5	81.25
8.		200	900	22000	4400	4400	3468.9	462.5	78.84
9.		300	600	19000	3800	5700	4415.7	496.1	76.53

3.7. Thomas model studies

The capacity of the adsorption in the fixed bed study and the constants of the Thomas model (q0 & Kth) have been examined by altering the inflow rate of the metal ion solution height of the adsorbent bed in the column and the concentration of metal ions like a breakthrough study. The Thomas model shows very high regression with the experimental conditions in the column study. The constants of the Thomas model and the inflow rate of the solution have been increased when the capacity of adsorption gets decreased (Uddin, 2017). Furthermore, the decrease in the concentration of metal ions increased the Thomas model constant (Kth), Due to the very high driving force in the higher concentrations of metal ions. During very high metal ion concentrations, this may lead to increases in the adsorption capacity and a similar trend also developed by varying the height of the adsorbent bed in the fixed bed column. The constants and regression values obtained from the Thomas model are represented in Tables 7–9 for Cr, Pb & Zn metal ions, respectively. Figures 14–16 show the graphical representation of Thomas model plots for the adsorption of Cr, Pb & Zn metal ions, respectively.

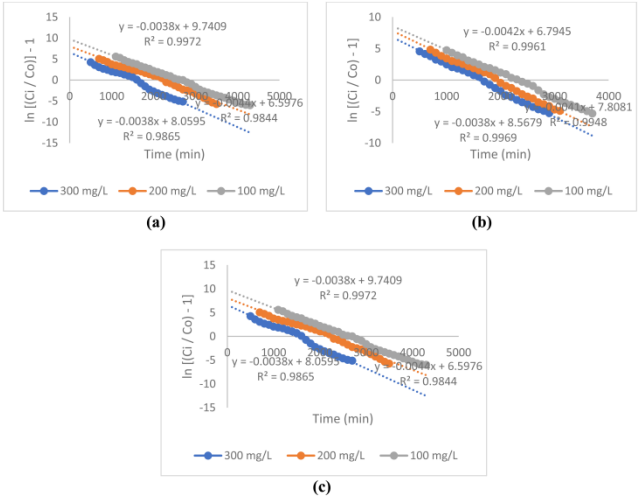

Figure 14. Thomas model plots in different Cr, Pb & Zn ion concentrations.

Table 7. Constants of Thomas model and parameters for Cr adsorption

S.No.	Slope	Intercept	C_0 (mg/L)	K_{th} (Min^{-1} mg^{-1} L)	Z (cm)	Q (mL/min)	q_0
1.	-0.0046	6.47	300	1.54×10^{-5}	5	5	387.45
2.	-0.00364	7.67	200	1.82×10^{-5}	5	5	342.83
3.	-0.00369	10.63	100	3.69×10^{-5}	5	5	251.28
4.	-0.00457	6.70	100	4.57×10^{-5}	5	5	238.26
5.	-0.00366	7.28	100	3.66×10^{-5}	7.5	5	264.83
6.	-0.00298	7.98	100	2.98×10^{-5}	10	5	287.32
7.	-0.00360	5.90	100	3.60×10^{-5}	5	5	253.24
8.	-0.00344	7.75	100	3.44×10^{-5}	5	7.5	225.47
9.	-0.00280	7.80	100	2.80×10^{-5}	5	10	198.26

Table 8. Constants of Thomas model and parameters for Pb adsorption

S.No.	Slope	Intercept	C_0 (mg/L)	K_{th} (Min^{-1} mg^{-1} L)	Z (cm)	Q (mL/min)	q_0
1.	-0.0044	6.59	300	1.46×10^{-5}	5	5	381.26
2.	-0.0037	8.05	200	1.85×10^{-5}	5	5	352.35
3.	-0.0037	9.74	100	3.70×10^{-5}	5	5	264.37
4.	-0.0040	6.53	100	4.0×10^{-5}	5	5	243.45
5.	-0.0037	7.59	100	3.70×10^{-5}	7.5	5	267.36
6.	-0.0035	8.68	100	3.50×10^{-5}	10	5	289.34
7.	-0.0035	5.72	100	3.50×10^{-5}	5	5	261.24
8.	-0.0036	7.73	100	3.60×10^{-5}	5	7.5	239.32
9.	-0.0030	8.10	100	3.0×10^{-5}	5	10	202.31

Table 9. Constants of Thomas model and parameters for Zn adsorption

S.No.	Slope	Intercept	C_0 (mg/L)	K_{th} (Min^{-1} mg^{-1} L)	Z (cm)	Q (mL/min)	q_0
1.	-0.0042	6.79	300	1.40×10^{-5}	5	5	380.54
2.	-0.0041	7.80	200	2.05×10^{-5}	5	5	327.43
3.	-0.0037	8.56	100	3.70×10^{-5}	5	5	264.24
4.	-0.0039	6.78	100	3.90×10^{-5}	5	5	232.54
5.	-0.0035	7.55	100	3.50×10^{-5}	7.5	5	258.43
6.	-0.0032	8.41	100	3.20×10^{-5}	10	5	272.74
7.	-0.0035	5.56	100	3.50×10^{-5}	5	5	256.46
8.	-0.0036	7.63	100	3.60×10^{-5}	5	7.5	235.24
9.	-0.0030	8.00	100	3.0×10^{-5}	5	10	204.56

Table 10. Constants of BDST model and parameters in different bed heights

S.No	Type of metal	Bed height (cm)	Conc. (mg/L)	C_i/C_o	Slope	Intercept	N_o (mg/L)	K (L/mg min)	R^2
1.	Cr	5	100	0.3	110	540	49050	4.5×10^{-5}	0.986
2.		7.5	100	0.4	100	918	53090	3.2×10^{-5}	0.986
3.		10	100	0.5	92	1733	57340	2.1×10^{-5}	0.994
4.	Pb	5	100	0.3	220	66	45930	1.9×10^{-5}	0.999
5.		7.5	100	0.4	160	743	51250	3.4×10^{-5}	0.997
6.		10	100	0.5	130	1525	54640	2.4×10^{-5}	0.982
7.	Zn	5	100	0.3	140	315	47560	3.7×10^{-5}	0.996
8.		7.5	100	0.4	122	1096	50540	3.3×10^{-5}	0.962
9.		10	100	0.5	104	1416	53650	2.2×10^{-5}	0.992

Table 11. Desorption rate of the adsorbent material in fixed bed column

S. No.	Type of Metal	Concentration of Sulfuric Acid	Final Concentration (mg/L)	Time (min)
1.	Chromium	0.1 N	740	30
		0.2 N	820	
		0.3 N	870	
2.	Lead	0.1 N	650	50
		0.2 N	710	
		0.3 N	780	
3.	Zinc	0.1 N	730	40
		0.2 N	780	
		0.3 N	850	

3.8. BDST model studies

In the fixed-bed column study, the adsorbent bed service time is the most important parameter for maximum adsorption efficiency. The Bed-Depth Service Time model helps to increase the amount of adsorption in the column by taking the constant metal ion concentration without any added experiments (Malik *et al.*, 2018). The main assumption of this model is that intra-particle diffusion and mass transfer resistance are insignificant. Also, it assumes that the major adsorption of metals occurred on the adsorbed bed surface (Ojedokun *et al.*, 2016). This model represents the relationship between the service time of the adsorbent and the height of the adsorbent bed. Referring to the assumptions of this model, for experimental work, 100 mg/L concentration of metal ion solutions were taken and allowed into the column with a flow rate of 5 mL/min by varying inlet and outlet concentrations. The linear relation was identified for service time and height of the bed by referring to Figure 17. The slope and intercept values were calculated based on the plots and represented in Table 10. The applicability of the BDST model with the fixed bed adsorption was identified through the linearity

and regression values (R^2>0.95). Also, there was an increase in the capacity of adsorption per unit volume of bed (No) with an increase in inlet and outlet (C_i & Co) concentrations due to the very high built-up of metal ions on the adsorbent surface. The least regression value was obtained at 50% of the inlet and outlet concentrations, and increased Ci & Co levels decreased the regression values. To obtain the earlier breakthrough, need a very high adsorbent bed with good condition inflow rate and metal ion concentration.

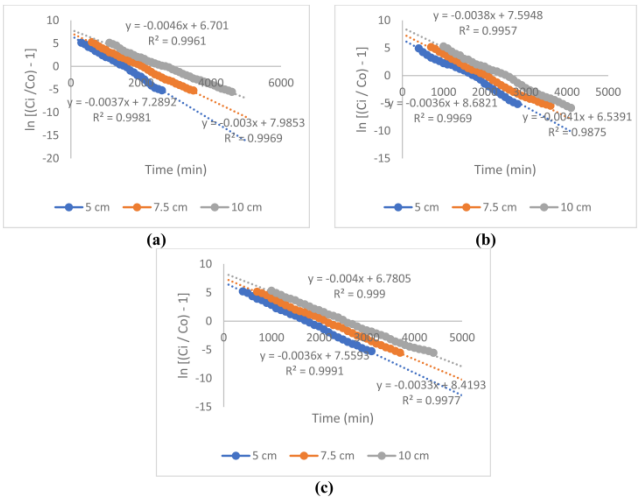

Figure 15. Thomas model plots in different bed depths for Cr, Pb & Zn metal ion adsorption.

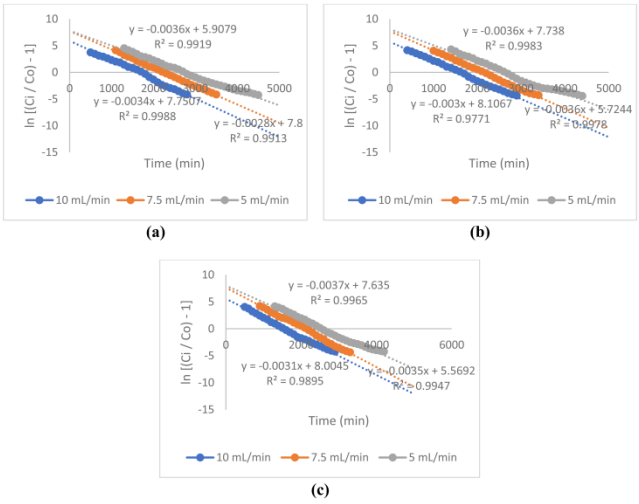

Figure 16. Thomas model plots in different inflow rate for Cr, Pb & Zn metal ion adsorption.

3.9. Impact of pH and its monitoring

The batch mode of studies was conducted using the rice husk powder by Priya *et al.*, 2022 and the optimum values from the batch mode of studies were taken for these experimental investigations. The metal ion concentration was fixed at 25 mg L^{-1} and rice husk powder dose was taken at 2.5 g L^{-1} with the temperature of the solution of 30°C. The pH of the solution was adjusted from 2.0 to 7.0 and its impact in adsorption efficiency of metal ion was shown in the Figure 18. It was seen that; the maximum amount of metal ion was adsorbed by the adsorbent at the pH of 2.0. When the pH of azo dye solution was increased, there was a decrease in metal ion uptake by the rice husk powder was observed.

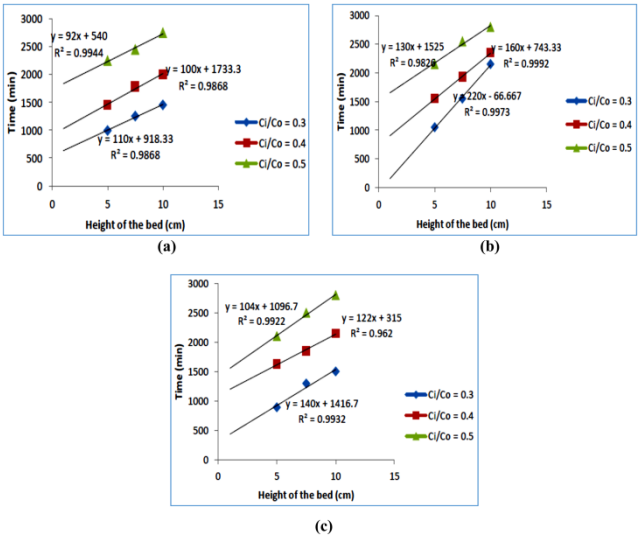

Figure 17. BDST plots of different inlet & outlet concentrations of Cr, Pb and Zn metal ion solutions

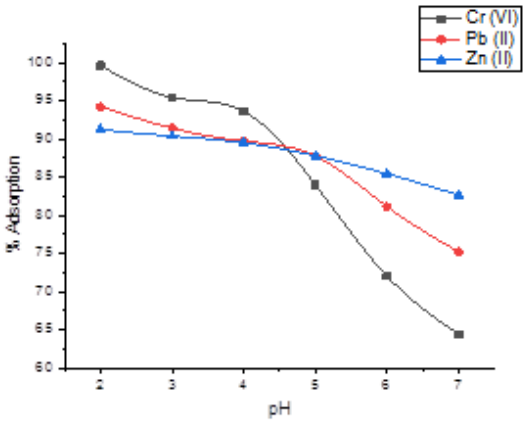

Figure 18. Impact of pH in metal ions adsorption.

3.10. Desorption & Regeneration

The desorption studies were conducted in a continuous flow mode using concentrated sulfuric acid (0.1N, 0.2N & 0.3N) in various concentrations. For this study, the flow rate of the metal ion solution in the fixed bed column was fixed at 5 mL/min, and the solution, after passing the adsorbent bed, was collected at the bottom of the column at 5 minutes interval. The elution curve of the fixed bed column is shown in Figure 19 for chromium, lead and zinc ion solutions. The trend has been seen that the desorption rate increases gradually up to the optimum level for the three different concentrations of sulfuric acid solutions. After that, the curve decreases the desorption rate (Menglu Sun *et al.*, 2018). This phenomenon is followed for all three metal ion solutions. Table 11 shows the maximum amount of desorption for Cr, Pb and Zn metal ions for various sulfuric ion concentrations. Reuse of spent adsorbent provides very good performance to the fixed bed column. Hence, the desorption- adsorption process

was conducted in three cycles up to their saturation level. Figure 20 shows the regeneration process up to cycles for Cr, Pb and Zn adsorption with 0.3 N of concentrated sulfuric acid.

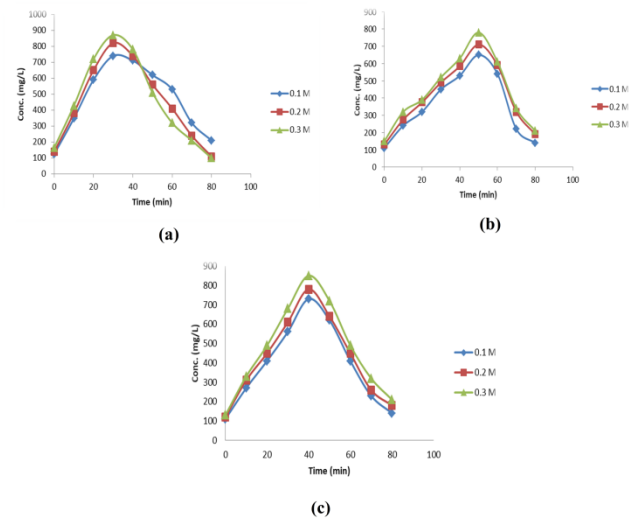

Figure 19. Desorption rate plots for Cr, Pb and Zn metal ions using H_2SO_4

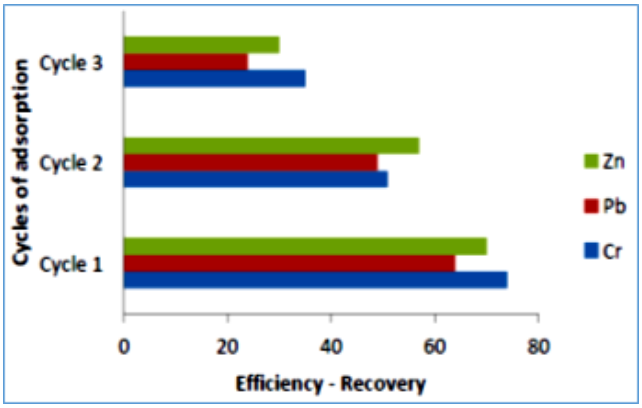

Figure 20. Regeneration of packed bed column.

4. Conclusion

A fixed-bed column study has evaluated the adsorption capacity of the iron oxide-coated rice husk powder nanoparticles for the metal ions (Cr, Pb & Zn) uptake from the aqueous solutions. SEM/EDX analysis confirms the presence of these heavy metal ions along with other organic pollutants. Various methods checked the stability of the prepared nano adsorbent, and the breakthrough time was also obtained under various conditions. The breakthrough curve attained the constant rate by the optimum bed height of 10 cm, concentrations of metal ions at 100 mg/L and inflow rate of metal ions containing solution at 5 mL/min. The Thomas and BDST models fitted well with the column adsorption studies with high regression values. The desorption and regeneration process were done by adding various concentrations of concentrated sulfuric acid to obtain a better performance of the fixed bed column. The maximum adsorption efficiency of 99.6 % for Cr, 75.21% for Pb and 82.63% for Zn metal ions was attained at an optimum pH of 2.0. The above experimental work concluded that the rice husk powder coated with iron oxides could adsorb the toxic pollutants from the aqueous medium.

References

Akpen G.D., Aho M.I., and Baba N. (2018). Adsorption of Cadmium (II) from simulated wastewater using albizia saman pod activated carbon in fixed bed columns. *Nigerian Journal of Technology*, **37**, 833–840.

Ali A., Saeed K., and Mabood F. (2016). Removal of chromium (VI) from aqueous medium using chemically modified banana peels as efficient low-cost adsorbent. *Alexandria Engineering Journal*, **55**, 2933–2942.

Barakat M.A. (2011). New trends in removing heavy metals from industrial wastewater. *Arabian Journal of Chemistry*, **4**, 361–377.

Buthelezi S.P., Olaniran A.O., and Pillay B. (2012). Textile dye removal from wastewater effluents using bioflocculants produced by indigenous bacterial isolates. *Molecules*, **17**, 14260–14274.

Chen X., Zhou S., Zhang L., You T., and Xu F. (2016). Adsorption of heavy metals by graphene oxide/cellulose hydrogel prepared from NaOH/urea aqueous solution. *Materials*, **9**, 582.

Edokpayi J.N., Odiyo J.O., Msagati T.A.M., and Popoola E.O. (2015). A Novel Approach for the Removal of Lead (II) Ion from Wastewater Using Mucilaginous Leaves of Diceriocaryum eriocarpum Plant, Sustainability, **7,** 14026 – 14041.

Fu F., and Wang Q. (2011). Removal of heavy metal ions from wastewaters: A review. *Journal of Environmental Management*, **92**, 407–418.

Goharshadi E.K., and Moghaddam M.B. (2015). Adsorption of hexavalent chromium ions from aqueous solution by graphene nanosheets: kinetic and thermodynamic studies. *International Journal of Environmental Science and Technology*, **12**, 2153–2160.

Guo T., Bulin C., Li B., Zhao Z., Yu H., Sun H., Ge X., and Xing R. (2018). Efficient removal of aqueous Pb (II) using partially reduced graphene oxide-Fe_3O_4. *Adsorption Science & Technology*, **36**, 1031–1048.

Hasfalina C.M., Maryam R.Z., Luqman C.A., and Rashid M. (2012). Adsorption of copper (II) from aqueous medium in fixed-bed column by Kenaf fibres. *APCBEE Procedia*, **3**, 255–263.

Hegazi H.A. (2013). Removal of heavy metals from wastewater using agricultural and industrial wastes as adsorbents. *HBRC Journal*, **9**, 276–282.

Itankar N., and Patil Y. (2013). Management of hexavalent chromium from industrial waste using low-cost waste biomass. *Procedia - Social and Behavioral Sciences*, **133**, 219–224.

Kara A., Üstün G.E., Solmaz S.K.A., and Demirbel E. (2013). Removal of Pb (II) ions in fixed-bed column from electroplating wastewater of bursa, an industrial city in Turkey. *Journal of Chemistry*, 953968.

Khulbe K.C. and Matsuura T. (2018). Removal of heavy metals and pollutants by membrane adsorption techniques. *Applied Water Science*, **8,** 19.

Lalitha L.M., and Mariraj S.M. (2018). Performance Evaluation of Multibed Adsorbent on Removal of Hexavalent chromium through various kinetic models. *Journal of Environmental Engineering and Landscape Management*, **26**, 285–298.

Malik D.S., Jain C.K., and Yadav A.K. (2018). Heavy metal removal by fixed-bed column – A review. *ChemBioEng Reviews*, **5**, 1–8.

Naddafi K., Nabizadeh R., Saeedi R., Mahvi A.H., Vaezi F., Yaghmaeian K., Ghasri A., and Nazmara S. (2007). Biosorption of lead (II) and cadmium (II) by protonated Sargassum glaucescens biomass in a continuous packed bed column. *Journal of Hazardous Materials*, **147**, 785–791.

Ojedokun A.T., and Bello O.S. (2016). Sequestering heavymetals from wastewater using cow dung. *Water Resources and Industry*, **13**, 7–13.

Owalude S.O. and Tella A.C. (2016). Removal of hexavalent chromium from aqueous solutions by adsorption on modified groundnut hull. *Beni-Surf University Journal of Basic and Applied Sciences*, **5**, 377–388.

Pan L., Wang Z., Yang Q., and Huang R. (2018). Efficient Removal of lead, copper and cadmium ions from water by a porous calcium alginate/graphene oxide composite aerogel. *Nanomaterials*, **8**, 957.

Pandey P.K., and Sharma S.K. (2017). Removal of Cr (VI) and Pb (II) from wastewater by ZeoliteNaX in fixed bed column. *Water Conservation Science and Engineering*, **2**, 61–65.

Priya A.K, Yogeshwaran V, Saravanan Rajendran, Tuan K.A. Hoang, Matias Soto-Moscoso, Ayman A. Ghfar and Chinna Bathula (2022), Investigation of mechanism of heavy metals (Cr^{6+}, Pb^{2+}& Zn^{2+}) adsorption from aqueous medium using rice husk ash: Kinetic and thermodynamic approach, *Chemosphere*, **286**, 131796.

Priya A.K., Yogeshwaran V., Rajendran S., Hoang T.H.A., Soto-Moscoso M., Ghfar A.A., and Bathula C. (2022). Investigation of mechanism of heavy metals (Cr^{6+}, Pb^{2+} & Zn^{2+}) adsorption from aqueous medium using rice husk ash: Kinetic and thermodynamic approach. *Chemosphere*, **286,** 131796.

Rai M.K., Shahi G., Meena V., Meena R., Chakraborty S., Singh R.S., and Rai B.N. (2016). Removal of hexavalent chromium Cr (VI) using activated carbon prepared from mango kernel activated with H_3PO_4. *Resource-Efficient Technologies*, **2**, S63–S70.

Sathish T., Vinithkumar N.V., Dharani G., and Kirubagaran R. (2015). Efficacy of mangrove leaf powder for bioremediation of chromium (VI) from aqueous solutions: kinetic and thermodynamic evaluation. *Applied Water Science*, **5,** 153–160.

Singha B., Naiya T.K., Bhattacharya A.K., and Das S.K. (2011). Cr (VI) ions removal from aqueous solutions using natural adsorbents—FTIR studies. *Journal of Environmental Protection*, **2**, 729–735.

Sukumar C., Janaki V., Vijayaraghavan K., Kamala-Kannan S., and Shanthi K. (2016), Removal of Cr (VI) using co-immobilized activated carbon and Bacillus subtilis: fixed-bed column study. *Clean Technologies and Environmental Policy*, ***19***, 251–258.

Sun M., Li P., Jin X., Ju X., Yan W., Yuan J., and Xing C. (2018). Heavy metal adsorption onto graphene oxide, amino group on magnetic nano adsorbents and application for detection of Pb (II) by strip sensor. *Food and Agricultural Immunology*, **29**, 1053–1073.

Taha S., Ricordel S., and Cisse I. (2011). Kinetic study and modeling of heavy metals removal by adsorption onto pea-nut husks incinerated residues. *Energy Procedia*, **6,** 143–152.

Tran L.T., Tran H.V., Le T.D., Bach G.L., and Tran L.D. (2019). Studying Ni (II) adsorption of magnetite/graphene oxide/chitosan nanocomposite. *Advances in Polymer Technology*, 8124351.

Uddin M.K. (2017). A review on the adsorption of heavy metals by clay minerals, with special focus on the past decade. *Chemical Engineering Journal*, **308**, 438–462.

Venkatraman Y., and Priya A.K. (2022). Removal of heavy metal ion concentrations from the wastewater using tobacco leaves coated with iron oxide nanoparticles. *International Journal of Environmental Science and Technology*, **19**, 2721–2736.

Wolowiec M., Komoroska–Kaufman M., Pruss A., Rzepa G. and Bajda T. (2019). Removal of heavy metals and metallaoids from water using drinking water treatment residuals ad adsorbents: A review, *Minerals*, **9**, 487.

Yogeshwaran V., and Priya A.K. (2021). Experimental studies on the removal of heavy metal ion concentration using sugarcane bagasse in batch adsorption process. *Desalination and Water Treatment*, **224**, 256–272.

Yunnen C., Ye W., Chen L., Lin G., Jinxia N., and Rushan R. (2017). Continuous fixed-bed column study and adsorption modeling: Removal of arsenate and arsenite in aqueous solution by organic modified spent grains. *Polish Journal of Environmental Studies*, **26**, 1847–1854.f